Table 5
Sequences of *cII* mutations in the liver of control Muta™Mouse

Mutant no.	Position	Mutation	Sequence			Amino acid change
A1	40	G to A	ATC	GAG	AGT	Glu to Lys
A2	205–213	−CGATTGGCG				Deletion
A3	34	C to T	CTA	CGA	ATC	Arg to Stop
A4	115	C to A	TCG	CAG	ATC	Gln to Lys
A5	212	C to T	TTG	GCG	CGA	Ala to Val
A6	89	C to A	ACA	GCG	GAA	Ala to Glu
A7	119–208	−ATGGCTCGAT				Deletion
A8	122	G to T	ATC	AGC	AGG	Ser to Ile
A9	233	T to C	ATT	CTC	ACC	Leu to Pro
A10	212	C to T	TTG	GCG	CGA	Ala to Val
A11[a]	89	C to A	ACA	GCG	GAA	Ala to Glu
A12	150	G to T	CCA	AAG	TTC	Lys to Asn
A13	205	C to T	GCT	CGA	TTG	Arg to Stop
A14	95	C to A	GAA	GCT	GTG	Ala to Asp
A15	89	C to T	ACA	GCG	GAA	Ala to Val
A16	212	C to T	TTG	GCG	CGA	Ala to Val
A17	122	G to T	ATC	AGC	AGG	Ser to Ile
A18[a]	150	G to T	CCA	AAG	TTC	Lys to Asn
A19	113	C to T	AAG	TCG	CAG	Ser to Leu
A20	210	G to T	CGA	TTG	GCG	Leu to Phe
A21	212	C to T	TTG	GCG	CGA	Ala to Val
A22	34	C to T	CTA	CGA	ATC	Arg to Stop
A23	110	A to T	GAT	AAG	TCG	Lys to Met
A24	241–246	−A	AAA	AAA	CGC	Frameshift
A25	196	G to A	GAC	GAC	ATG	Asp to Asn
A26[a]	34	C to T	CTA	CGA	ATC	Arg to Stop
A27	107	A to C	GTT	GAT	AAG	Asp to Ala
A28	89	C to T	ACA	GCG	GAA	Ala to Val
A29	196	G to A	GAC	GAC	ATG	Asp to Asn
A30	212	C to T	TTG	GCG	CGA	Ala to Val
A31	3	G to A	–	ATG	GTT	Met to Ile
A32	179–184	−G	TGG	GGG	GTC	Frameshift
A33	95	C to G	GAA	GCT	GTG	Ala to Gly
A34	110	A to C	GAT	AAG	TCG	Lys to Thr
A35[a]	89	C to T	ACA	GCG	GAA	Ala to Val
A36[a]	110	A to C	GAT	AAG	TCG	Lys to Thr

[a] Ascribable to the same mutation obtained in an identical mouse.

and 42 induced mutants of 4,10-DAC in the respective two organs. The mutations are characterized in Tables 2–9 and summarized in Tables 10 and 11. In Tables 10 and 11, the same mutations from an identical mouse were treated as a single event.

In the liver, spontaneous mutations consisted mainly of G:C to A:T transitions (14/30) followed by G:C to T:A transversions (7/30) as shown in the previous report on the *cII* mutant spectrum in the liver of control Muta™Mouse [9,26].

The majority of chrysene-induced mutations were G:C to T:A transversions (13/36), followed by the G:C to A:T transitions (9/36). Both 1,10-DAC- and 4,10-DAC-induced mutations also consisted mainly of G:C to T:A transversions (17/38 and 18/38, respectively). The *cII* mutant spectra by all the test compounds in the lung showed a tendency similar to those in the liver.

4. Discussion

1,10-DAC and 4,10-DAC, the tetracyclic azaPAHs and diaza-analogs of chrysene, could not be converted to the bay-region diol epoxide form because of their nitrogen atoms in the benzene rings of the bay-region

Table 6
Sequences of *cII* mutations in the lung of 1,10-DAC-treated Muta™Mouse

Mutant no.	Position	Mutation	Sequence			Amino acid change
c1	163–164	CT to AA	CTG	CTT	GCT	Leu to Asn
c2	215	G to C	GCG	CGA	CAA	Arg to Pro
c3	132	G to T	TGG	AAG	AGG	Lys to Asn
c4	79	G to T	ACT	GAG	AAG	Glu to Stop
c5	160–161	CT to AG	ATG	CTG	CTT	Leu to Arg
c6	178	T to A	ATG	CTG	CTT	Trp to Arg
c7	100–101	GG to AT	GTG	GGC	GTT	Gly to Ile
c8	65	C to A	ATC	GCA	ATG	Ala to Glu
c9	150	G to T	CCA	AAG	TTC	Lys to Asn
c10[a]	79	G to T	ACT	GAG	AAG	Glu to Stop
c11	132	G to T	TGG	AAG	AGG	Lys to Asn
c12	34	C to T	CTA	CGA	ATC	Arg to Stop
c13	140	G to C	GAC	TGG	ATT	Trp to Ser
c14	179–184	−G	TGG	GGG	GTC	Frameshift
c15	212	C to T	TTG	GCG	CGA	Ala to Val
c16	141	G to T	GAC	TGG	ATT	Trp to Cys
c17	62	T to C	AAA	ATC	GCA	Ile to Thr
c18	196	G to T	GAC	GAC	ATG	Asp to Tyr
c19	212	C to G	TTG	GCG	CGA	Ala to Gly
c20	42	G to T	ATC	GAG	AGT	Glu to Asp
c21	160	C to A	ATG	CTG	CTT	Leu to Met
c22	215	G to C	GCG	CGA	CAA	Arg to Pro
c23	127	T to G	AGG	TGG	AAG	Trp to Gly
c24	64	G to T	ATC	GCA	ATG	Ala to Ser
c25	100	G to A	GTG	GGC	GTT	Gly to Ser
c26	111	G to T	GAT	AAG	TCG	Lys to Asn
c27	62	T to G	AAA	ATC	GCA	Ile to Ser
c28	196	G to T	GAC	GAC	ATG	Asp to Tyr
c29	179–184	−G	TGG	GGG	GTC	Frameshift
c30	122	G to T	ATC	AGC	AGG	Ser to Ile
c31	126	G to C	AGC	AGG	TGG	Arg to Ser
c32	128	G to T	AGG	TGG	AAG	Trp to Leu
c33	161	T to A	ATG	CTG	CTT	Leu to Gln
c34	129	G to T	AGG	TGG	AAG	Trp to Cys
c35	179–184	−G	TGG	GGG	GTC	Frameshift
c36	164–165	−T	CTG	CTT	GCT	Frameshift
c37	150	G to T	CCA	AAG	TTC	Lys to Asn
c38	178	T to G	GAA	TGG	GGG	Trp to Gly
c39	167	C to G	CTT	GCT	GTT	Ala to Gly
c40	106	G to T	GTT	GAT	AAG	Asp to Tyr
c41	51	G to C	GCG	TTG	CTT	Leu to Phe
c42	133	A to T	AAG	AGG	GAC	Arg to Trp
c43	169	G to C	GCT	GTT	CTT	Val to Leu

[a] Ascribable to the same mutation obtained in an identical mouse.

epoxide or diol moiety. Nevertheless, 1,10-DAC and 4,10-DAC showed in vitro mutagenicity in the Ames tests using rat liver S9 or human liver microsomes in our previous study [17]. Therefore, these DACs might be converted to ultimate mutagenic forms by a mechanism different from that of chrysene. We have investigated the in vivo mutagenicity of some aza-PAHs, such as quinoline and 10-azaBaP [5,8–10,15]. The 1,10-DAC and 4,10-DAC consist of two quinoline moieties and also have a structure similar to 10-azaBaP. In the present study, we attempted to investigate the in vivo mutagenicity of DACs compared with chrysene

Table 7
Sequences of *cII* mutations in the lung of 4,10-DAC-treated Muta™Mouse

Mutant no.	Position	Mutation	Sequence			Amino acid change
d1	123	C to A	ATC	AGC	AGG	Ser to Arg
	138	C to A	AGG	GAC	TGG	Asp to Glu
d2	29	C to A	GAG	GCT	CTA	Ala to Asp
d3	117	G to T	TCG	CAG	ATC	Gln to His
d4	212	C to T	TTG	GCG	CGA	Ala to Val
d5	125	G to T	AGC	AGG	TGG	Arg to Met
d6	160	C to A	ATG	CTG	CTT	Leu to Met
d7	128	G to T	AGG	TGG	AAG	Trp to Leu
d8	293	G to T	TTC	TGA	–	Stop to Leu
d9	220	G to T	CAA	GTT	GCT	Val to Phe
d10	57	C to A	CTT	AAC	AAA	Asn to Lys
d11	111	G to T	GAT	AAG	TCG	Lys to Asn
d12	115	C to A	TCG	CAG	ATC	Gln to Lys
d13	51	G to T	GCG	TTG	CTT	Leu to Phe
d14	179–184	−G	TGG	GGG	GTC	Frameshift
d15	115	C to T	TCG	CAG	ATC	Gln to Stop
d16	88	G to C	ACA	GCG	GAA	Ala to Pro
d17	132	G to T	TGG	AAG	AGG	Lys to Asn
d18	117	G to T	TCG	CAG	ATC	Gln to His
d19	65	C to A	ATC	GCA	ATG	Ala to Glu
d20[a]	115	C to A	TCG	CAG	ATC	Gln to Lys
d21[a]	88	G to C	ACA	GCG	GAA	Ala to Pro
d22	145	C to G	ATT	CCA	AAG	Pro to Ala
d23	103	G to T	GGC	GTT	GAT	Val to Phe
d24	167	C to G	CTT	GCT	GTT	Ala to Gly
d25	212	C to G	TTG	GCG	CGA	Ala to Gly
d26	163	C to T	CTG	CTT	GCT	Leu to Phe
d27	224	C to A	GTT	GCT	GCG	Ala to Asp
d28	175	G to T	CTT	GAA	TGG	Glu to Stop
d29	40	G to A	ATC	GAG	AGT	Glu to Lys
d30	160	C to A	ATG	CTG	CTT	Leu to Met
d31[a]	103	G to T	GGC	GTT	GAT	Val to Phe
d32	89	C to T	ACA	GCG	GAA	Ala to Val
d33	179–184	−G	TGG	GGG	GTC	Frameshift
d34	95	C to A	GAA	GCT	GTG	Ala to Asp
d35	134	G to T	AAG	AGG	GAC	Arg to Met
d36	101	G to T	GTG	GGC	GTT	Gly to Val
d37	34	C to T	CTA	CGA	ATC	Arg to Stop
d38	129	G to T	AGG	TGG	AAG	Trp to Cys
d39	89	−C	ACA	GCG	GAA	Frameshift
d40	125	G to T	AGC	AGG	TGG	Arg to Met
d41	65	C to A	ATC	GCA	ATG	Ala to Glu
d42	122	G to T	ATC	AGC	AGG	Ser to Ile

[a] Ascribable to the same mutation obtained in an identical mouse.

to understand the nature of the in vivo mutagenicity of azaPAHs.

Table 12 summarizes the in vivo mutagenicity of a series of azaPAHs with the pyridine moiety, investigated in our previous and present studies using Muta™Mouse. One of the authors (T.S.) reported that the median toxic dose (TD_{50}) of chemicals as used for numerical description of their carcinogenic potency is well correlated with in vivo mutagenic potency, which was calculated by division of the chemical-induced mutant frequency by the total injection dose of the chemical in the transgenic mouse [27]. We calculated

Table 8
Sequences of *cII* mutations in the lung of chrysene-treated Muta™Mouse

Mutant no.	Position	Mutation	Sequence			Amino acid change
b1	112	T to C	AAG	TCG	CAG	Ser to Pro
b2	89	C to T	ACA	GCG	GAA	Ala to Val
b3	34	C to T	CTA	CGA	ATC	Arg to Stop
b4	141	G to A	GAC	TGG	ATT	Trp to Stop
b5	94	G to C	GAA	GCT	GTG	Ala to Pro
b6	126	G to C	AGC	AGG	TGG	Arg to Ser
b7	214	C to T	GCG	CGA	CAA	Arg to Stop
b8[a]	34	C to T	CTA	CGA	ATC	Arg to Stop
b9	190–198	−GAC	GAC	GAC	GAC	Deletion
b10	106	G to T	GTT	GAT	AAG	Asp to Tyr
b11	113	C to A	AAG	TCG	CAG	Ser to Stop
b12	101	G to T	GTG	GGC	GTT	Gly to Val
b13	122	G to T	ATC	AGC	AGG	Ser to Ile
b14	196	G to T	GAC	GAC	ATG	Asp to Tyr
b15[a]	113	C to A	AAG	TCG	CAG	Ser to Stop
b16[a]	190–198	−GAC	GAC	GAC	GAC	Deletion
b17	34	C to T	CTA	CGA	ATC	Arg to Stop
b18	215	G to C	GCG	CGA	CAA	Arg to Pro
b19	113	C to T	AAG	TCG	CAG	Ser to Leu
b20	233	T to A	ATT	CTC	ACC	Leu to His
b21	104	T to G	GGC	GTT	GAT	Val to Gry
b22	42	G to T	ATC	GAG	AGT	Glu to Asp
b23	25	G to T	AAC	GAG	GCT	Glu to Stop
b24	117	G to T	TCG	CAG	ATC	Gln to His
b25	233	−T	ATT	CTC	ACC	Frameshift
b26	123	C to G	ATC	AGC	AGG	Ser to Arg
b27	169	G to C	GCT	GTT	CTT	Val to Leu
b28[a]	215	G to C	GCG	CGA	CAA	Arg to Pro
b29	155	C to T	TTC	TCA	ATG	Ser to Leu
b30	26	A to G	AAC	GAG	GCT	Glu to Gly
b31	34	C to T	CTA	CGA	ATC	Arg to Stop
b32	40	G to A	ATC	GAG	AGT	Glu to Lys
b33	117	G to T	TCG	CAG	ATC	Gln to His
b34	179–184	−G	TGG	GGG	GTC	Frameshift
b35	163	C to A	CTG	CTT	GCT	Leu to Ile
b36	150	G to T	CCA	AAG	TTC	Lys to Asn
b37	94	G to C	GAA	GCT	GTG	Ala to Pro
b38	221	T to C	CAA	GTT	GCT	Val to Ala
b39	73	G to A	CTT	GGA	ACT	Gly to Arg

[a] Ascribable to the same mutation obtained in an identical mouse.

the mutagenic activity by the following formula to compare the mutagenicity between azaPAHs:

fold-increase in *lacZ* MF (%) = *lacZ* MF obtained by test chemical/spontaneous *lacZ* MF × 100.
Mutagenic activity = fold-increase in *lacZ* MF/total dose of test chemical.

The organs given in capital letters in Table 12 indicate those that showed significant mutation and those given in small letters indicate negative organs. The underlined organs are those which showed the highest increase in *lacZ* MF. When the test chemical induced mutation in multiple organs, the mutagenic activity was calculated using the data of the underlined organs.

Although the five azaPAHs tested in our previous reports (quinoline, benzo[*f*]quinoline, benzo[*h*]quinoline, 1,7-phenanthroline and 10-azaBaP) induced mutation only in the specific organ such as the liver, 1,10-DAC and 4,10-DAC showed significant mutant frequencies in all of the six organs examined and the

Table 9
Sequences of *cII* mutations in the lung of control Muta™Mouse

Mutant no.	Position	Mutation	Sequence			Amino acid change
a1	146	C to T	ATT	CCA	AAG	Pro to Leu
a2	196	G to A	GAC	GAC	ATG	Asp to Asn
a3	113	C to T	AAG	TCG	CAG	Ser to Leu
a4	217	C to T	CGA	CAA	GTT	Gln to Stop
a5	180	G to A	GAA	TGG	GGG	Trp to Stop
a6	73	G to A	CTT	GGA	ACT	Gly to Arg
a7	132	G to T	TGG	AAG	AGG	Lys to Asn
a8	58–61	−A	AAC	AAA	ATC	Frameshift
a9	241–246	−A	AAA	AAA	CGC	Frameshift
a10	149–164	−AGTTCTCAATGCTGCT				Deletion
a11	25	G to T	AAC	GAG	GCT	Glu to Stop
a12	214	C to T	GCG	CGA	CAA	Arg to Stop
a13	197	A to G	GAC	GAC	ATG	Asp to Gly
a14	111	G to T	GAT	AAG	TCG	Lys to Asn
a15	206	G to C	GCT	CGA	TTG	Arg to Pro
a16	212	C to T	TTG	GCG	CGA	Ala to Val
a17	38	T to G	CGA	ATC	GAG	Ile to Ser
a18	40	G to A	ATC	GAG	AGT	Glu to Lys
a19[a]	40	G to A	ATC	GAG	AGT	Glu to Lys
a20	34	C to T	CTA	CGA	ATC	Arg to Stop
a21	90–91	GG to T	GCG	GAA	GCT	Frameshift
a22	113	C to T	AAG	TCG	CAG	Ser to Leu
a23	140	G to A	GAC	TGG	ATT	Trp to Stop
a24	110	A to T	GAT	AAG	TCG	Lys to Met
a25	175	G to A	CTT	GAA	TGG	Glu to Lys
a26	172	C to T	GTT	CTT	GAA	Leu to Phe
a27	89	C to T	ACA	GCG	GAA	Ala to Val
a28[a]	34	C to T	CTA	CGA	ATC	Arg to Stop
a29	221	T to G	CAA	GTT	GCT	Val to Gly
a30	273–275	ACA to CGATGCACG				Insertion
a31	212	C to T	TTG	GCG	CGA	Ala to Val
a32	193	G to A	GAC	GAC	GAC	Asp to Asn
a33	34	C to T	CTA	CGA	ATC	Arg to Stop
a34	31	C to G	GCT	CTA	CGA	Leu to Val
a35	155	C to A	TTC	TCA	ATG	Ser to Stop
a36	128	G to A	AGG	TGG	AAG	Trp to Stop
a37	88	G to T	ACA	GCG	GAA	Ala to Ser
a38[a]	34	C to T	CTA	CGA	ATC	Arg to Stop

[a] Ascribable to the same mutation obtained in an identical mouse.

highest *lacZ* mutant frequency in the lung. Chrysene also significantly induced mutation in all of the six organs examined, although chrysene showed similar mutant frequencies in all the six organs. These results suggest that nitrogen substitution in the chrysene skeleton may enhance the inducibility of mutation in the mouse lung.

4,10-DAC showed the highest mutagenic activity, followed in order by: quinoline > 1,7-phenenthroline ≈ 1,10-DAC > benzo[*h*]quinoline ≈ 10-azaBaP = benzo[*f*]quinoline. The number of mutagenic activity of chrysene is the same as that of benzo[*f*]quinoline, which shows the lowest mutagenic activity among the series of azaPAHs tested. The 4,10-DAC gave mutant frequencies higher than 1,10-DAC in all the test organs and the increase in *lacZ* MF obtained by 4,10-DAC is more than twice that by 1,10-DAC in most of the organs tested. Therefore, these results suggest that the nitrogen-substituted position affects the strength of mutagenicity of the DAC structure.

Table 10
Summary of *cII* mutation spectra in the liver of Muta™Mouse

Mutation class	Control (%)	1,10-DAC (%)	4,10-DAC (%)	Chrysene (%)
Total	30 (100)	38 (100)	38 (100)	36 (100)
Base substitution	26 (87)	35 (92)	35 (92)	32 (89)
Transitions				
GC to AT	14 (47)	7 (18)	8 (21)	9 (25)
AT to GC	1 (3)	2 (5)	0 (0)	2 (6)
Transversions				
AT to TA	1 (3)	3 (8)	1 (3)	2 (6)
AT to CG	2 (7)	1 (3)	1 (3)	1 (3)
GC to TA	7 (23)	17 (45)	18 (47)	13 (36)
GC to CG	1 (3)	5 (13)	7 (18)	5 (14)
−1 Frameshifts	2 (7)	1 (3)	1 (3)	3 (8)
+1 Frameshifts	0 (0)	0 (0)	0 (0)	0 (0)
Deletion	2 (7)	1 (3)	0 (0)	1 (3)
Insertion	0 (0)	0 (0)	0 (0)	0 (0)
Complex	0 (0)	1 (3)	2 (5)	0 (0)

The same mutations from an identical mouse were counted as a single event.

We further attempted *cII* mutant spectrum analysis in the liver and lung, which were shown to give the highest *lacZ* mutant frequencies by chrysene and DACs, respectively. In both organs, the spontaneous mutations consisted mainly of G:C to A:T transitions and the mutant spectrum in the control Muta™Mice showed no difference between the liver and lung. The G:C to A:T transitions in the control mice are likely to be ascribable to the deamination of 5-methylcytosine at the CpG site as previously reported [28]. DACs predominantly induced the G:C to T:A transversion in both organs. It was especially noteworthy that there was no difference in the *cII* mutant spectrum of 4,10-DAC between the lung and liver in spite of the quantitative difference showed by 4,10-DAC with its 3.9-fold higher *cII* mutant frequency in the lung than in the liver. These results suggest that the high mutagenicity in the lung of 4,10-DAC-treated mice might not arise from

Table 11
Summary of *cII* mutation spectra in the lung of Muta™Mouse

Mutation class	Control (%)	1,10-DAC (%)	4,10-DAC (%)	Chrysene (%)
Total	35 (100)	41 (100)	39 (100)	35 (100)
Base substitution	30 (86)	34 (83)	35 (90)	32 (91)
Transitions				
GC to AT	19 (54)	3 (7)	6 (15)	10 (29)
AT to GC	1 (3)	1 (2)	0 (0)	3 (9)
Transversions				
AT to TA	1 (3)	3 (7)	0 (0)	1 (3)
AT to CG	2 (6)	3 (7)	0 (0)	1 (3)
GC to TA	5 (14)	16 (39)	25 (64)	11 (31)
GC to CG	2 (6)	8 (20)	4 (10)	6 (17)
−1 Frameshifts	2 (6)	4 (10)	3 (8)	2 (6)
+1 Frameshifts	0 (0)	0 (0)	0 (0)	0 (0)
Deletion	1 (3)	0 (0)	0 (0)	1 (3)
Insertion	0 (0)	0 (0)	0 (0)	0 (0)
Complex	2 (6)	3 (7)	1 (3)	0 (0)

The same mutations from an identical mouse were counted as a single event.

Table 12
In vivo mutagenicity of a series of aza-PAHs

Chemical	Total dose (mg/kg)	Tested organ[a]							Mutagenic activity[b]	Sequence analysis	Ref.
Quinoline	250	LIVER	spleen	lung	kidney	bm	testis		1.76	Increase of GC to CG	[8–10]
Benzo[*f*]quinoline	400	LIVER	spleen	lung	kidney	bm			0.37	Featureless	[15]
Benzo[*h*]quinoline	400	liver	spleen	LUNG	kidney	bm			0.45	Featureless	[15]
1,7-Phenanthroline	200	LIVER	spleen	lung	kidney	bm			1.14	Increase of GC to CG	[15]
10-azaBaP	625	LIVER	spleen	lung	kidney	bm	COLON	gs fs	0.39	Featureless	[5]
1,10-DAC	400	LIVER	SPLEEN	LUNG	KIDNEY	BM	COLON		1.08	Increase of GC to TA	From this study
4,10-DAC	800	LIVER	SPLEEN	LUNG	KIDNEY	BM	COLON		2.32	Increase of GC to TA	From this study
Chrysene	800	LIVER	SPLEEN	LUNG	KIDNEY	BM	COLON		0.37	Increase of GC to TA	From this study

Superscript (c) in footnote (b) stands for fold-increase in *lacZ* MF (%) = *lacZ* MF obtained by test chemical/spontaneous *lacZ* MF × 100.
[a] The organs in capital letters are those that showed significant induction of mutation and those in small letters indicate negative organs. The underlined organ showed the highest increase in *lacZ* MF. BM(bm), bone marrow; gs, glandular stomach; fs, forestomach.
[b] Mutagenic activity = fold-increase in *lacZ* MF[c]/total dose of test chemical.

the increase of organ-specific adduct(s). In our previous studies, quinoline and 1,7-phenenthroline induced the G:C to C:G transversion [9]. On the other hand, 1,10-DAC and 4,10-DAC induced the G:C to T:A transversion. These results suggest that the enlargement of the molecular size in azaPAHs might change the major mutation pattern from the G:C to C:G transversion to the G:C to T:A transversion. Chrysene also increased the G:C to T:A transversion like DACs. Therefore, it was suggested that the nitrogen substitution in the chrysene skeleton may give no influence on the mutation spectrum.

We have previously reported that quinoline, a partial structure of DACs and one of simplest azaPAHs, showed mutagenicity in both in vitro [14,29] and in vivo [8] and that metabolic activation of quinoline might take place in the pyridine moiety to form the ultimate genotoxic form, an enamine epoxide (1,4-hydrated 2,3-epoxide) [10–14]. Moreover, benzo[*h*]quinoline and 1,7-phenanthroline, tricyclic azaPAHs with the quinoline moiety as a partial structure, may be activated in the pyridine moiety to show the mutagenicity as reported in our previous paper [16]. DACs, which consist of two quinoline moieties as a partial structure, might be also converted to the enamine epoxide structure in the pyridine moiety to be able to induce mutation. We are trying to investigate further to clarity the metabolic activation pathway of DACs.

In conclusion, it is suggested that the two types of nitrogen substitution in the chrysene structure enhances the mutagenicity in the mouse lung, although they have no influence on the organ specificity and mutation spectrum.

Acknowledgements

We thank Dr. T. Nohmi for his kind gift of *E. coli*, NM759 and BHB2688 and Dr. K. Masumura for his technical direction in making packaging extracts. This research is supported in part by the grant from Ministry of the Environment, Japan.

References

[1] Y. Kitahara, H. Okuda, K. Shudo, T. Okamoto, M. Nagao, Y. Seino, T. Sugimura, Synthesis and mutagenicity of 10-

azabenzo[*a*]pyrene-4,5-oxide and other pentacyclic aza-arene oxides, Chem. Pharm. Bull. 26 (1978) 1950–1953.
[2] C.H. Ho, B.R. Clark, M.R. Guerin, B.D. Barkenbus, T.K. Rao, J.L. Epler, Analytical and biological analysis of test materials from the synthetic fuel technologies, Mutat. Res. 85 (1981) 335–345.
[3] D.M. Jerina, R.E. Lehr, H. Yagi, O. Hernandez, P.M. Dansette, P.G. Wislocki, A.W. Wood, R.L. Chang, W. Levin, A.H. Conney, Mutagenicity of benzo[a]pyrene derivatives and the description of a quantum mechanical model which predict the ease of carbonium ion formation from diol epoxides, in: F.J. de Serres, J.R. Fouts, J.R. Bend, R.W. Philpot (Eds.), In vitro Metabolic Activation in Mutagenesis Testing, Elsevier-North Holland Biochem. Press, Amesterdam, 1976, pp. 159–177.
[4] A.W. Wood, R.L. Chang, W. Levin, D.E. Ryan, P.E. Thomas, H.D. Mah, J.M. Karle, H. Yagi, D.M. Jerina, A.H. Conney, Mutagenicity and tumorigenicity of phenanthrene and chrysene epoxides and diol epoxides, Cancer Res. 39 (1979) 4069–4077.
[5] K. Yamada, T. Suzuki, A. Kohara, M. Hayashi, A. Hakura, T. Mizutani, K. Saeki, Effect of 10-aza-substitution on benzo[*a*]pyrene mutagenicity in vivo and in vitro, Mutat. Res. 521 (2002) 187–200.
[6] K. Hirao, Y. Shinohara, H. Tsuda, S. Fukushima, M. Takahashi, Carcinogenic activity of quinoline on rat liver, Cancer Res. 36 (1976) 329.
[7] Y. Shinohara, T. Ogiso, M. Hananouchi, K. Nakanishi, T. yoshimura, N. Ito, Effect of various factors on the induction of liver tumors in animals by quinoline, Jpn. J. Cancer Res. 68 (1977) 785–796.
[8] T. Suzuki, Y. Miyata, K. Saeki, Y. Kawazoe, M. Hayashi, T. Sofuni, In vivo mutagenesis by the hepatocarcinogen quinoline in the *lacZ* transgenic mouse: evidence for its in vivo genotoxicity, Mutat. Res. 412 (1998) 161–166.
[9] T. Suzuki, X. Wang, Y. Miyata, K. Saeki, A. Kohara, Y. Kawazoe, M. Hayashi, T. Sofuni, Hepatocarcinogen quinoline induces G:C to C:G transversions in the *cII* gene in the liver of lambda/*lacZ* transgenic mice (MutaMouse), Mutat. Res. 456 (2000) 73–81.
[10] Y. Miyata, K. Saeki, Y. Kawazoe, M. Hayashi, T. Sofuni, T. Suzuki, Antimutagenic structure modification of quinoline assessed by an in vivo mutagenesis assay using *lacZ*-transgenic mice, Mutat. Res. 414 (1998) 165–169.
[11] M. Tada, K. Takahashi, Y. Kawazoe, N. Ito, Binding of quinoline to nucleic acid in a subcellular microsomal system, Chem. Biol. Interact. 29 (1980) 257–266.
[12] M. Tada, K. Takahashi, Y. Kawazoe, Metabolites of quinoline, a hepatocarcinogen, in a subcellular microsomal system, Chem. Pharm. Bull. 30 (1982) 3834–3837.
[13] K. Takahashi, M. Kamiya, Y. Sengoku, K. Kohda, Y. Kawazoe, Deprivation of the mutagenic property of quinoline: inhibition of mutagenic metabolism by fluorine substitution, Chem. Pharm. Bull. 36 (1988) 4630–4633.
[14] K. Saeki, K. Takahashi, Y. Kawazoe, Metabolism of mutagenicity-deprived 3-fluoroquinoline: comparison with mutagenic quinoline, Biol. Pharm. Bull. 16 (1993) 232–234.
[15] K. Yamada, T. Suzuki, A. Kohara, M. Hayashi, T. Mizutani, K. Saeki, In vivo mutagenicity of benzo[*f*]quinoline, benzo[*h*]quinoline, and 1,7-phenanthroline using the *lacZ* transgenic mice, Mutat. Res. 559 (2004) 83–95.
[16] K. Saeki, H. Kawai, Y. Kawazoe, A. Hakura, Dual stimulatory and inhibitory effects of fluorine-substitution on mutagenicity: an extension of the enamine epoxide theory for activation of the quinoline nucleus, Biol. Pharm. Bull. 20 (1997) 646–650.
[17] K. Yamada, A. Hakura, T. Kato, T. Mizutani, K. Saeki, Nitrogen substitution effects on the mutagenicity and cytochrome P450 isoform-selectivity of chrysene analogs, Mutat. Res., in press.
[18] S.V. Nekrasov, A.V. El'tsov, Polynuclear aza-aromatic compounds, I. Zh. Org. Khim. 7 (1971) 188–199.
[19] W.C. Summers, P.M. Glazer, D. Malkevich, Lambda phage shuttle vectors for analysis of mutations in mammalian cells in culture and in transgenic mice, Mutat. Res. 220 (1989) 263–268.
[20] E.J. Gunther, N.E. Murray, P.M. Glazer, High efficiency, restriction-deficient in vitro packaging extracts for bacteriophage lambda DNA using a new *E.coli* lysogen, Nucleic Acids Res. 21 (1993) 3903–3904.
[21] J.A. Gossen, A.C. Molijn, G.R. Douglas, J. Vijg, Application of galactose-sensitive *E. coli* strains as selective hosts for *LacZ*-plasmids, Nucleic Acids Res. 20 (1992) 3254.
[22] S.W. Dean, B. Myhr, Measurement of gene mutation in vivo using Muta Mouse and positive selection for *lacZ*-phage, Mutagenesis 9 (1994) 183–185.
[23] J. Jiao, G.R. Douglas, J.D. Gingerich, L.M. Soper, Comparison of the molecular characteristics of *lacZ* transgenic mouse mutations detected by visual and positive selection, Mutat. Res. 372 (1996) 141–145.
[24] J.L. Jakubczak, G. Merlino, J.E. French, W.J. Muller, B. Paul, S. Adhya, S. Garges, Analysis of genetic instability during mammary tumor progression using a novel selection-based assay for in vivo mutations in a bacteriophage lambda transgene target, Proc. Natl. Acad. Sci. U.S.A. 93 (1996) 9073–9078.
[25] Collaborative Study Group on the Transgenic Mutation assay (CSGTM), Organ variation in the mutagenicity of ethylnitrosourea in Muta mouse: results of the collaborative study on the transgenic mutation assay by JEMS/MMS, Environ. Mol. Mutagen., 28 (1996) 363–375.
[26] H. Ikehata, M. Takatsu, Y. Saito, T. Ono, Distribution of spontaneous CpG-associated G:C → A:T mutations in the lacZ gene of Muta mice: effects of CpG methylation, the sequence context of CpG sites, and severity of mutations on the activity of the *lacZ* gene product, Environ. Mol. Mutagen. 36 (2000) 301–311.
[27] T. Suzuki, An evaluation of the transgenic mouse mutation assays, Environ. Mutagen. Res. 25 (2003) 119–125.
[28] R. Holliday, G.W. Grigg, DNA methylation and mutation, Mutat. Res. 285 (1993) 61–67.
[29] T. Kato, K. Saeki, Y. Kawazoe, A. Hakura, Effects of oligofluorine substitution on the mutagenicity of quinoline: a study with twelve fluoroquinoline derivatives, Mutat. Res. 439 (1999) 149–157.

Proteomics 2005, *5*, 4287–4295 DOI 10.1002/pmic.200401287

REGULAR ARTICLE

Proteomic analysis of sera from hepatocellular carcinoma patients after radiofrequency ablation treatment

Takayuki Kawakami[1], Yujin Hoshida[1], Fumihiko Kanai[1, 2], Yasuo Tanaka[1], Keisuke Tateishi[1], Tsuneo Ikenoue[1, 3], Shuntaro Obi[1], Shinpei Sato[1], Takuma Teratani[1], Shuichiro Shiina[1], Takao Kawabe[1], Takayoshi Suzuki[4], Naoya Hatano[5], Hisaaki Taniguchi[6] and Masao Omata[1, 2]

[1] Department of Gastroenterology, Graduate School of Medicine, Faculty of Medicine, University of Tokyo, Tokyo, Japan
[2] Clinical Research Center, University of Tokyo Hospital, Tokyo, Japan
[3] Division of Gastroenterology, The Institute for Adult Disease, Asahi Life Foundation, Tokyo, Japan
[4] Division of Cellular and Gene Therapy Products, National Institute of Health Science, Tokyo, Japan
[5] Department of Cell Physiology, Kagawa University, Faculty of Medicine, Kagawa, Japan
[6] Posttranslational Modification and Dynamic Regulation Research Team, RIKEN Harima Institute, Hyogo, Japan

Comparative proteomic analysis was used to search for characteristic alterations in the sera of hepatocellular carcinoma (HCC) patients who had undergone curative radiofrequency ablation treatment. Serum samples collected from eight patients before and after treatment were subjected to 2-DE. Eighty-eight protein spots differentially expressed with the treatment were selected by clustering analysis, and the proteins were identified by MS based on MALDI-TOF/TOF analysis and public database searches. The statistical analysis suggested that four proteins decreased after treatment (pro-apolipoprotein, α2-HS glycoprotein, apolipoprotein A-IV precursor, and PRO1708/PRO2044, which is the carboxy terminal fragment of albumin) and that seven proteins were increased after treatment, including leucine-rich α2-glycoprotein and α1-antitrypsin. These data facilitate the identification of differentially expressed proteins that are involved in HCC carcinogenesis and provide candidate biomarkers for the development of diagnostic and therapeutic tools.

Received: September 6, 2004
Revised: February 9, 2005
Accepted: February 11, 2005

Keywords:
2-DE / Hepatocellular carcinoma / Serum proteome

1 Introduction

The current methods for the diagnosis of hepatocellular carcinoma (HCC) rely on serological markers, such as alpha-fetoprotein (AFP) and certain liver enzymes, together with physical assessments and imaging technologies (*e.g.*, ultrasound and computed tomography) [1]. Increases in the serum levels of des-gamma-carboxyprothrombin (DCP) and the fucosylated isoform of AFP have also been associated with HCC. Nevertheless, particularly in hepatitis B virus (HBV) infection, a diagnosis of HCC is sometimes made when the disease is too far advanced for effective treatment, and thus the 5-year survival rates are very low [2]. Clearly, better methods for screening and early diagnosis are important for improved prognosis.

Radiofrequency ablation treatment (RFA) has recently been introduced in the therapeutic modality of HCC [3]. Assuming that the tumor is diagnosed as HCC at an early stage, *i.e.*, at a tumor diameter of less than 3 cm and with restricted growth in several nodules, it can be curatively treated with RFA. In RFA treatment, heat is generated locally

Correspondence: Dr. Fumihiko Kanai, Department of Gastroenterology, Graduate School of Medicine, Faculty of Medicine, University of Tokyo, 7-3-1 Hongo, Bunkyo-ku, Tokyo 113-8655, Japan
E-mail: kanaif-int@h.u-tokyo.ac.jp
Fax: + 81-3-5800-8775

Abbreviations: AFP, alpha-fetoprotein; **AHSG**, alpha-2-HS glycoprotein; **DCP**, des gamma carboxyprothrombin; **HBV**, hepatitis B virus; **HCC**, hepatocellular carcinoma; **HCV**, hepatitis C virus; **RFA**, radiofrequency ablation therapy; **TAE**, transcatheter arterial embolization

by a high-frequency alternating current that flows from the electrodes. A probe is inserted into the lesion in the liver and local heat is generated to melt the tissue adjacent to the probe, causing tissue coagulative necrosis. In the case of RFA, as compared with percutaneous ethanol injection therapy [3, 4], the area of necrosis can be controlled precisely by adjusting the duration of the radiofrequency emission, which increases concentrically from the electrode. Because RFA can shorten the period of hospitalization, it is rapidly gaining popularity as a treatment modality for HCC in Japan and elsewhere [5].

In an effort to identify protein markers that have pathological significance for various cancers, proteomic analysis with 2-DE and MS has been used. Presently, proteomic analysis is widely used for the molecular analysis of various tumors and for the identification of new targets for cancer therapy [6, 7]. Proteomic analysis of disease is based on the profiling of the differential expression levels of various proteins between healthy and diseased states. Thus, identified disease markers may be involved in the etiology of the disease. Recently, two groups applied proteomic analysis to the sera of HBV-infected patients in a search for serological biomarkers of the disease [8, 9]. They found that apolipoprotein AI was associated with the HBV-infected status or HCC of HBV-infected patients. In order to identify candidate biomarkers, they used a 2-DE gel separation technique and MALDI-TOF MS. These findings are attributable to the development of MS/MS. Moreover, one of the latest advances in the accurate, sensitive resolution of mass is TOF/TOF technology [10, 11]. Therefore, in the present study, we used the new high-resolution MALDI-TOF/TOF mass spectrometer (Applied Biosystems), in combination with gel-based proteomic analysis, to profile the proteins in the sera of HCC patients. Eight pairs of pre- and post-treatment serum samples were analyzed for alterations in protein expression.

2 Materials and methods

2.1 Materials

Eight human serum samples were collected with the informed consent of patients with HCC, who had been admitted to the University of Tokyo Hospital. The samples were analyzed in accordance with procedures approved by the ethics committee of the hospital. The collection interval after treatment was 1 wk.

CHAPS, DTT, SDS, iodoacetamide, TEMED, ammonium bicarbonate, Tris, glycine, methanol, urea, and TFA of HPLC grade were purchased from Wako Pure Chemicals (Osaka, Japan). The IEF system (IPGphore), Immobiline DryStrips (18 cm, pH 4–7), and Protein A-Sepharose Fast Flow were purchased from Amersham Pharmacia (Little Chalfont, Buckinghamshire, UK). Acrylamide was obtained from Bio-Rad (Hercules, CA, USA). The MS experiments were carried out in a AB4700 MALDI-TOF/TOF mass spectrometer (Applied Biosystems, Framingham, MA, USA). A 99% grade CHCA was purchased from Sigma-Aldrich (St. Louis, MO, USA), sequence-grade trypsin was obtained from Promega (Madison, WI, USA), and the standard peptide mixture used for calibration was from Applied Biosystems.

2.2 Sample preparation

Each serum sample of 200 μL was absorbed with 200 μL volume of Protein A-Sepharose Fast Flow, which had been previously equilibrated with sodium phosphate buffer (pH 7.1). After the flow-through fractions were collected, the resin was washed with an equal volume of sodium phosphate buffer (pH 7.1), and each wash solution was collected, together with the previously described flow-through fraction. The protein concentration was estimated using Bradford reagent (Bio-Rad), and the samples were stored at −80°C until use.

2.3 2-DE and gel staining

IEF was carried out with 18-cm, pH 4–7 IPG strips according to the manufacturer's instructions, with minor modifications. The 2-DE gels were run on two separate occasions for each sample. The IPG strips were located in the IPG ceramic holders and rehydrated overnight with 300 μg of the sample, which was solubilized in 340 μL of a solution that contained 8 M Urea, 2% CHAPS, 18.3 mM DTT, 0.5% v/v IPG buffer (pH 4–7), and a trace of bromophenol blue. The proteins were separated by the IEF system using a programmed voltage gradient at 20°C. After overnight rehydration, the voltage was set at 500 V for 1 h, increased to 4000 V with a 3-h linear gradient, and then increased further to 8000 V for 5.5 h. The samples were maintained at 8000 V until a total run of 47.5 kVh was accomplished (about 9.5 h in total). After IEF, the strips were equilibrated for 15 min in 10 mL of equilibration buffer (6 M Urea, 2% SDS, 0.05 M Tris-HCl (pH 8.8), 30% glycerol, 1% DTT) and then transferred for a further 15 min into equilibration buffer that contained 2.5 iodoacetamide instead of DTT. The equilibrated IPG strips were transferred onto 12.5% uniform second-dimensional polyacrylamide gels, and electrophoresis was carried out in vertical uniform slab SDS-PAGE at 30 mA per gel for about 4.5 h. Each gel measured 20 × 18 cm. Protein spots in the gels were visualized by silver staining using conventional protocols [12], with minor modifications. Briefly, the gels were fixed overnight in 40% ethanol and 10% acetic acid in water. After the gels were washed twice with 30% ethanol in water, they were incubated for exactly 1 min in 0.05% w/v NaS_2O_3. The gels were then washed twice with water for 20 s each and incubated for 20 min in 0.2% w/v $AgNO_3$. The gels were washed three times for 20 s each in water and developed with 3% w/v Na_2CO_3 in 0.05% v/v formaldehyde in water until the desired contrast was reached (usually after 2.5 min). The reaction was stopped by the addition of 0.5% acetic acid and incubation for 20 min.

2.4 Gel image and data analyses

After silver staining, the 2-DE gels were scanned with an ES-2200 image scanner (Epson, Tokyo, Japan). The intensity of each spot was calculated in ppm using the PDQuest software (Bio-Rad). The volume of each spot was normalized for the total density of the gel. To exclude spots that showed variable intensity in duplicated experiments, we calculated the SD of each spot; spots that showed deviations of more than 2 × SD and spots with missing values in over 25% of the samples were eliminated (Fig. 2) [13]. The averages of the intensity values from duplicate experiments for the remaining 812 spots were used for further analysis. Agglomerative hierarchical clustering of protein spots was performed using the Cluster and TreeView programs (http://rana.lbl.gov/EisenSoftware.htm) [14]. The changes in spot intensities after RFA treatment were evaluated using the *t*-statistic. The level of statistical significance was determined by the random permutation test with false discovery rate correction. Corrected *p* values less than 0.05 were considered significant.

2.5 In-gel digestion

Protein spots were excised from gels as 1 × 1-mm pieces and were digested with trypsin using a previously published procedure [15, 16], which was modified as described in this section. Gel slices were destained in a 1:1 solution of 30 mM potassium ferricyanide and 100 mM sodium thiosulfate, and then washed with water. After the addition of ACN and complete drying in a SpeedVac®, the gels were reswollen in 2 μL of trypsin solution (20 μg/mL in 25 mM ammonium bicarbonate) and 0.1% *n*-octyl glucoside. After the solvents had penetrated into the gels, 10 μL of 25 mM ammonium bicarbonate that contained 0.1% *n*-octyl glucoside was added, and the mixture was incubated at 37°C overnight. After in-gel digestion with trypsin, the tryptic peptides were extracted, first with 50 μL and then with 25 μL of extraction buffer (50% ACN/0.1% TFA). The supernatants were collected and dried in the SpeedVac®, and the samples were dissolved in 25 μL of 0.1% TFA.

2.6 Data examination and protein identification

Using ZipTip® μC18, the tryptic peptides were desalted and concentrated, and then eluted with 1 μL of matrix solution (5 mg/mL CHCA in 50% ACN/0.1% TFA) onto a MALDI-TOF/TOF 2 × 96-well target plate. MS/MS analysis was performed on a model 4700 Proteomics Analyzer (Applied Biosystems), and air was used as the collision gas. The spectra were obtained by the accumulation of 2000–3500 consecutive laser shots.

Proteins that were expressed differentially in the pre- and post-treatment samples were analyzed by MALDI-TOF, which permitted the identification of peptide masses for subsequent MS/MS analysis. Spectrum peak harvesting and baseline correction were carried out automatically. The query was made for all species, with the minimum number of matched masses being set at four. The maximum tolerance level for the peptide masses was 50 ppm, and the modifications accepted were carbamidomethyl cysteines and artifactual oxidation of methionines. The NCBI non-redundant databases were used for the searches, and the MS/MS studies were carried out with the same parameters as those described previously for the PMF research, using the MASCOT PMF search tools (Matrix Science, London, UK; http://www.matrixscience.com/search_form_select.html). The precursor peak error was set at 2 Da, and fragment tolerance was defined as 0.6 Da. Internal calibration of the MS/MS data was not performed.

2.7 Western blotting

Western blotting was performed as described previously [17]. Three paired samples were separated on 10–20% gradient SDS-PAGE and transferred onto PVDF membranes. The membranes were blocked with 100% Block Ace (Dainippon Pharmaceutical, Osaka, Japan) at 4°C overnight and incubated with sheep anti-AHSG antibody (ab8939) (Abcam, Cambridgeshire, UK) in TBST that contained 10% Block Ace at 4°C overnight. The membranes were washed and incubated with horseradish peroxidase-conjugated secondary antibodies, followed by chemiluminescence detection according to the manufacturer's instructions (Amersham Biosciences).

3 Results

3.1 Sample preparation and gel image analysis

We characterized the proteomic serum patterns of eight HCC patients following treatment with RFA or RFA plus transcatheter arterial embolization (TAE). A total of 16 serum samples (before and after treatment for eight patients) were analyzed by 2-DE; an image of a 2-DE gel is shown in Fig. 1. The clinical characteristics of the patients are shown in Table 1. Eight of the patients were infected with HBV or HCV and suffered from HCC (maximum diameter 3.2 cm). These patients were treated with curative RFA or curative RFA plus TAE. The changes in the levels of the HCC markers (AFP/L3/DCP), owing to the therapeutic procedure, are indicated in Table 1 (before *vs.* after treatment).

The serum samples were first prepared using Protein A-Sepharose Fast Flow beads to deplete the immunoglobulins, which are proteins that are abundant in the serum. Another abundant serum protein, albumin, was not depleted from the samples in this study, as albumin is also a carrier protein that conveys a large variety of compounds, including hormones, lipoproteins, and amino acids [18, 19]. Therefore, the removal of albumin from serum might result in the specific removal of low-abundance cytokines, peptide hormones, and lipoproteins of interest [20].

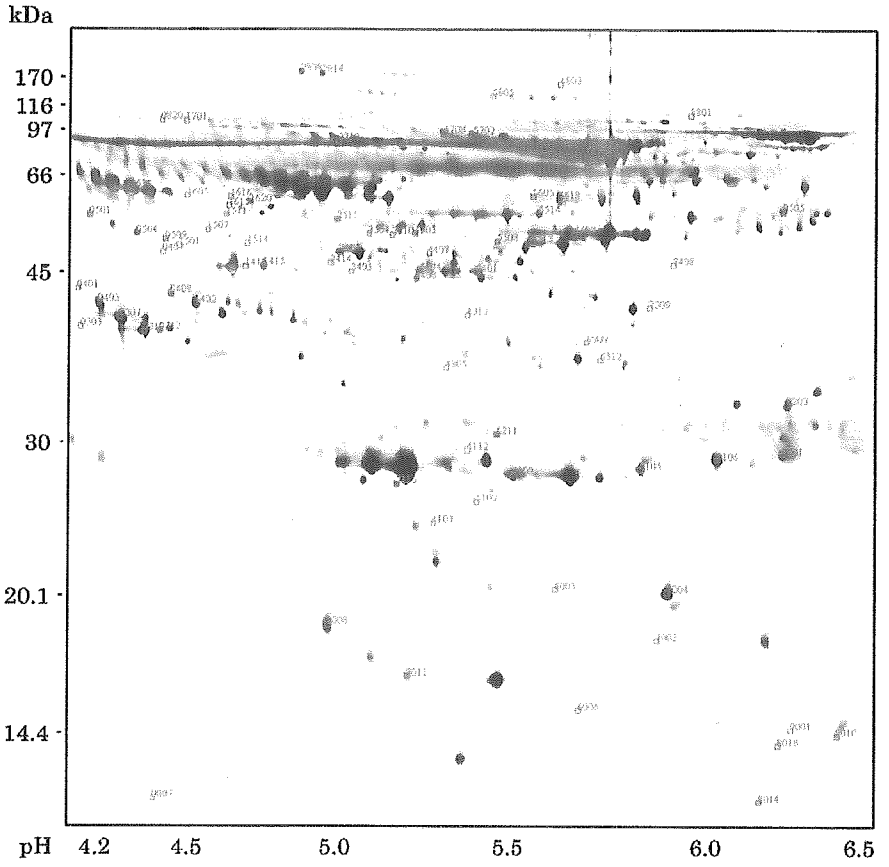

Figure 1. Serum protein patterns on a 2-DE gel (12.5%) after the removal of immunoglobulin. The 2-DE running conditions are described in the text. Protein (300 μg) was loaded onto the IEF gel strip (pH 4–7). Following 2-DE separation, the protein spots were visualized by silver staining and were numbered using the PDQuest software. A representative gel image is shown.

Table 1. Profiles of patients. Eight cases infected with hepatitis virus with HCC were enrolled in this analysis. Second column is TNM staging and max size of hepatocellular carcinoma(cm). TNM is tumor staging system, which uses three criteria to judge the stage of the cancer – primary tumor(T), rigional lymph nodes(N), and distant metastasis(M) – stage I through IV. AFP, L3 and DCP are HCC tumor markers, which are often clinically used. L3 fraction is a fucosylated AFP subtype and more specific for HCC than AFP. If TAE was done, it was stated in the last column

	cases	TNM/radius	changes by the treatment			
			AFP (IU/L)	L3 (%)	DCP (IU/L)	
1.	70F C-LC	II/ϕ 1,4 cm	7 ⇒ 7	N.D.	18 ⇒ 16	
2.	81M C-CH	I/ϕ 1,2 cm	32 ⇒ 29	2.0 ⇒ 0.5	13 ⇒ 15	
3.	64M C-CH	II/ϕ 2,1 cm	11 ⇒ 12	0.5 ⇒ 0.5	13 ⇒ 14	
4.	56F B-LC	II/ϕ 3,0 cm	162 ⇒ 55	43.3 ⇒ 33.2	10 ⇒ 10	TAE(+)
5.	74F C-LC	III/ϕ 2,9 cm	8855 ⇒ 912	5.2 ⇒ 7.0	134 ⇒ 16	TAE(+)
6.	55F B-CH	II/ϕ 3,2 cm	7 ⇒ 5	N.D.	59 ⇒ 18	TAE(+)
7.	58M C-LC	I/ϕ 1,5 cm	195 ⇒ 132	12.0 ⇒ 5.3	12 ⇒ 13	
8.	64F C-CH	II/ϕ 3,0 cm	1375 ⇒ 108	1.7 ⇒ 2.4	24 ⇒ 13	TAE(+)

TAE: transarterial embolization, N.D.: not detected

In order to ensure reproducibility, the 2-DE pattern of each patient serum sample was analyzed in two separate experiments. The image analysis showed that these 2-DE maps were similar, as shown in Fig. 1. Using the PDQuest image analysis software, 1133 spots were resolved on the 2-DE gels.

After excluding spots with intensities that varied by over 2 SD in duplicate gels (Fig. 2), hierarchical clustering

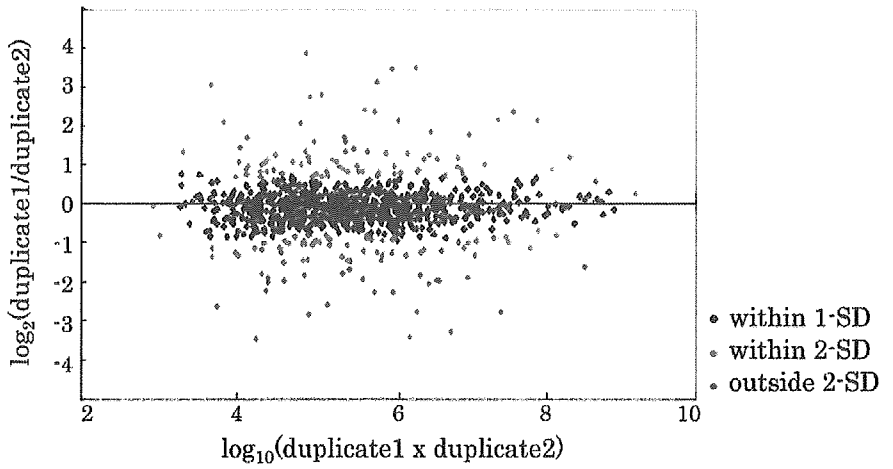

Figure 2. Reproducibility of 2-DE-based protein spot quantification. The spot intensity-dependent SD was calculated based on the ratio-intensity plot, using the data from duplicate experiments. Protein spots with intensities that varied by >2 × SD between experiments were eliminated from the subsequent analysis.

was performed with the remaining 812 spots. As shown in Fig. 3A, the unsupervised clustering analysis demonstrated that each pair of samples before and after RFA treatment lined up side by side, except in case 2, which means that the treatment did not produce any drastic change in the protein abundance in common across the eight patients. We may have missed subtle changes that could be associated with the tumor. Therefore, we divided the serum samples into two groups, *i.e.*, before and after treatment, and performed supervised clustering analysis to discover proteins expressed differentially with the treatment. Of 812 protein spots, 88 protein spots were selected as changing significantly in this analysis (Fig. 3B).

3.2 Protein identification of spots

The 88 protein spots shown in Fig. 3B were subjected to in-gel trypsin digestion and MS, and 45 protein spots (51%) were identified. Many of these identified spots represented PTM variants; they were collapsed into 11 distinct proteins after homology and similarity searches to eliminate redundant protein annotations. Although 15 protein spots are shown in Table 2 and Fig. 3B (asterisks), they still contain PTM variants. The remaining differential protein spots were not identified at this point, because the spot intensities were too faint to obtain sufficient amounts of tryptic peptide for protein identification. Several spots were identified by MALDI-TOF/TOF analysis.

The levels of four proteins were decreased after RFA: PRO1708/PRO2044 (the C-terminal fragment of albumin), pro-apolipoprotein, α2-HS glycoprotein (AHSG), and apolipoprotein A-IV precursor (Table 2 and Fig. 4A). The levels of seven proteins were increased after treatment: leucine-rich α2-glycoprotein, α1-antitrypsin, macroglobulin α2, haptoglobin (precursor), serum paraoxonase, complement C3 precursor, and C4A (Fig. 4B).

3.3 Western blotting with the anti-AHSG antibody

The expression of AHSG was confirmed by Western blot analysis with the anti-AHSG antibody. Paired sera from the patients were dissolved in SDS-PAGE gel buffer and blotted onto PVDF membranes. As shown in Fig. 5, the AHSG protein level was decreased after RFA treatment in three of six patients.

4 Discussion

Chronic infection with HBV or HCV is a significant risk factor for the development of HCC [18, 19]. The monitoring of disease progression and the prediction of outcome currently depend on a combination of physical and serological assessments. Unfortunately, these methods often lack the sensitivity required to detect HCC at an early stage, when therapeutic options are the most effective, especially when all three of the HCC markers AFP, L3 (fucosylated fraction of AFP), and DCP, are within normal ranges. There is a very real need for the discovery of markers that can detect the disease at an earlier stage in a higher proportion of patients and that are suitable for screening populations known to be at high risk for the development of HCC.

In the search for new biomarkers, several groups have analyzed differences in the levels of RNA expressed in normal and tumor-derived liver tissues [21–24] or in cultured cells [22, 25–27]. Similarly, some groups have studied differences in the protein profiles, or proteomes, of normal and tumor-derived liver tissues, cell lines, and serum [8, 9]. These studies have provided new insights into tumor carcinogenesis. For the discovery of disease progression markers that can be used for HCC patient screening, it is desirable to uncover changes in specific gene products that can be found in samples, such as serum, that are easily collected from patients.

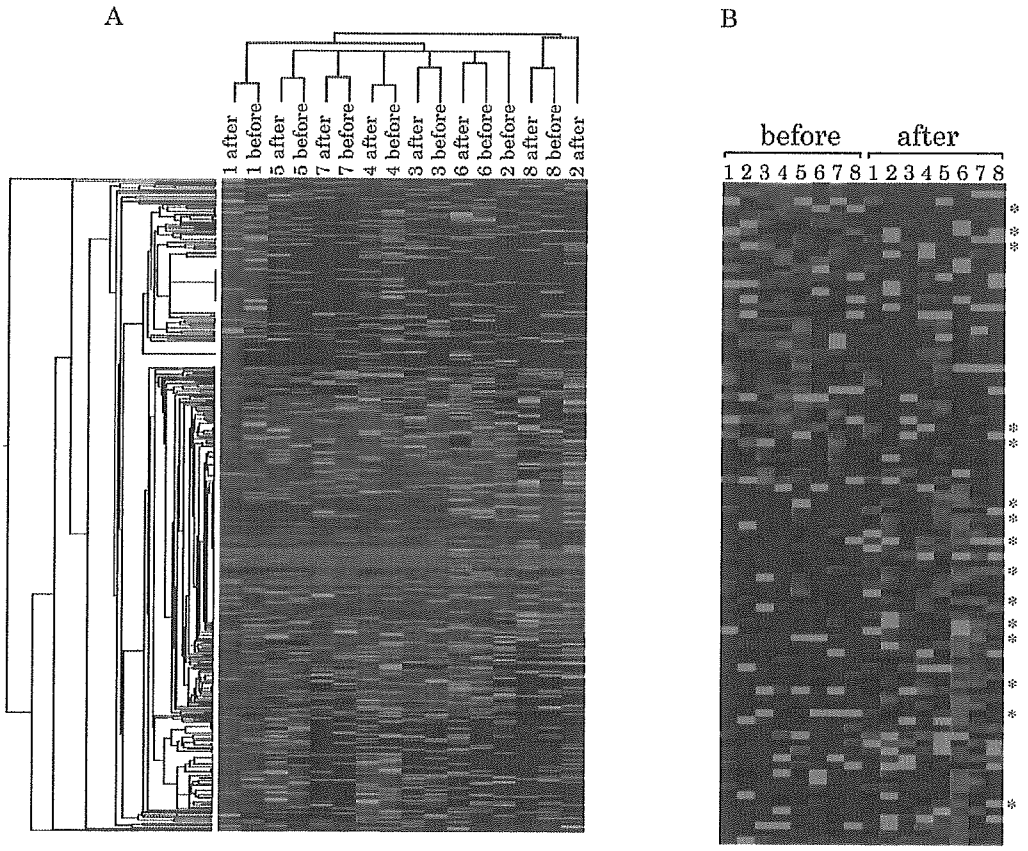

Figure 3. Hierarchical clustering analysis of serum protein spots. (A) Unsupervised clustering of eight cases and 812 spots. (B) Eighty-eight protein spots that were expressed differentially before and after treatment for HCC were selected in the supervised clustering analysis. Of these, 45 protein spots were identified using MS. The 15 spots indicated by asterisks (also listed in Table 2) still contain variants modified post-translationally, and the final number of proteins that changed with treatment is 11. Gray: missing value.

Table 2. Identified proteins by mass spectrometry. 2-DE gel images were analyzed by PDQuest software and detected spots were numbered (Spot no.). The values of score, M_r and p*I* are indicated in MASCOT MS/MS Ion search. The ratio between before and after treatment is indicated as Ratio (before/after). The scaling factor of the spot intensity used in PDQuest software is PPM (parts per million) and Mean and SE (standard error) of each spot was calcurated. Corrected p values <0.05 were considered to be significant. Right panel is the heat map extracted from the Fig. 3 of each protein. The line order is as same as Table 2.

Spot no.	Protein identified	Accesion no.	Score	Ratio (before/after)	Mr (kDa)	pI	Mean	SE
9010	PRO1708 /PRO2044	gi|7959791 /gi6650826	62	3.65	29.2	7.0	2467	433
3115	proapolipoprotein	gi|178775	124	2.08	28.9	5.5	1112	251
638	alpha2-HS glycoprotein	gi|2521981	180	1.44	35.6	5.2	5882	629
1605	alpha2-HS glycoprotein	gi|2521981	30	1.39	35.6	5.2	190	34
3401	apolipoprotein A-IV precursor	gi|178779	109	2.33	43.4	5.2	990	205
501	leucine-rich α-2-glycoprotein	gi|72059	63	0.44	34.3	5.7	1365	209
504	leucine-rich α-2-glycoprotein	gi|16418467	37	0.54	38.2	6.5	1520	169
2808	alpha-1-antitrypsin	gi|177831	68	0.52	46.7	5.4	1145	196
8801	macroglobulin α2	gi|224053	115	0.61	160.7	6.0	323	32
6003	haptoglobin Hp2	gi|223976	154	0.55	41.7	6.2	5235	1036
2414	haptoglobin precursor	gi|306882	106	0.52	45.2	6.1	2966	2349
1507	serum paraoxonase	gi|130675	112	0.41	39.7	5.1	2470	576
1514	serum paraoxonase	gi|130675	112	0.43	39.7	5.1	6798	1798
1412	complement C3 precursor	gi|4557385	129	0.41	187.1	6.0	459	231
4207	complement C4A	gi|443671	158	0.54	193.5	6.8	525	97

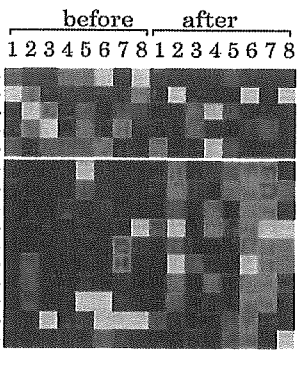

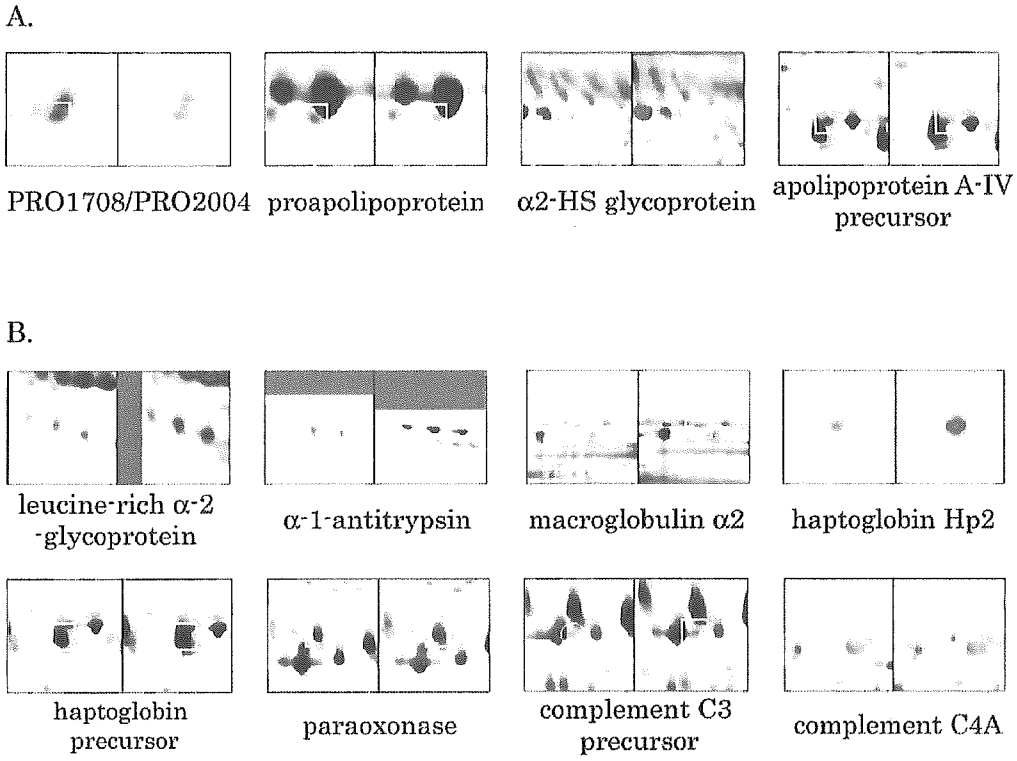

Figure 4. Identification of spots that exhibited changed levels in response to HCC treatment. (A) Identified spots with decreased levels after treatment. PRO1708/PRO2204 is the C-terminal fragment of albumin. (B) Identified spots with increased levels after treatment. Each spot is enclosed in a square, and representative gels images are shown.

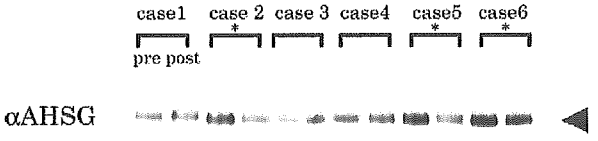

Figure 5. Western blot using the anti-AHSG antibody. Sera were run on a 10–20% gel. The Western blot shows that, in cases 2, 5, and 6, the levels of AHSG were higher before treatment than after treatment.

Steel *et al.* [9] properly dealt with the variability between individuals by combining an equal mass of total serum protein from individuals to form a composite sample for each of the four groups and by comparing the composite 2-DE gels of the four groups. As shown in Table 1, we lacked sufficient samples to detect significant differences, and the patients had different etiological backgrounds. We tried to minimize the variance between individuals by comparing paired gels derived from the same patient's serum. The constituents of serum after treatment must be the same as those before treatment, except for tumor-associated proteins or the consequences of treatment, in order to compare serum samples from the same patient. The timing of serum collection after treatment is important for comparative analysis, and we collected the post-treatment sera 1 wk after treatment, at the time of discharge from hospital. We considered this period of time reasonable in the clinical setting.

As described in Section 2, we collected serum samples before and after HCC treatment. At the time of discharge, the transaminases (ALT/AST) were unchanged or slightly upregulated from before treatment (the ratios of after/before were between 0.9 and 2; data not shown). It was not practical to wait for 1 month for all the serological parameters to stabilize and the tumor makers to decrease markedly in some cases, as shown in Table 1. Thus we considered 1 wk a reasonable interval and carefully continued our analyses, introducing a statistical analysis to eliminate artifactual errors.

In this study, we identified four proteins that had decreased levels following HCC treatment (Table 2). None of these proteins has been reported to be associated with liver cancer. Apolipoprotein A-IV (precursor) is synthesized primarily in the intestine [28, 29] and is secreted in the plasma; because its expression is suppressed in the sera of HBV-infected individuals, it is assumed to be an indicator of HBV infection [9]. AHSG, which is also known as human fetuin, is a liver secretory glycoprotein found at high levels in the serum and mineralized bone. This protein has the char-

acteristics of a negative acute-phase protein, in that the serum concentrations decrease significantly after major surgical procedures, trauma, burns, and severe inflammation. Western blotting with the anti-AHSG antibody confirmed that the serum level of AHSG was decreased by HCC treatment (Fig. 5). The protein with the most significant change in abundance was PRO1708/PRO2044 (Table 2). This protein is the C-terminal part of albumin. However, it was spotted in a very different location from albumin (the M_r and p*I* values of PRO1708/PRO2044 are 29 kDa and 7.6, respectively, whereas those of albumin are 69 kDa and 6.0 in 2-DE gels). We postulated that the partial fragment had a special physiological meaning; therefore, we used PRO1708/PRO2044 instead of a fragment of albumin in the text and table.

PRO1708/PRO2044 and AHSG were upregulated in the sera of HCC patients, as compared with levels in HCC-eradicated sera. Although the levels of AHSG may fluctuate as a result of liver damage or inflammation, it is not clear why the levels of the other proteins decrease after treatment. These results suggest roles for these proteins in HCC, but further confirmatory studies are necessary.

The levels of seven different proteins were elevated after HCC treatment. The increases in the levels of these proteins may be attributable to acute stress reactions or leakage from damaged liver tissues. Serum haptoglobin levels are widely used to study various liver diseases and are reported to be linked to liver damage in HBV liver infection [9]. Liver injury caused by RFA treatment may have increased the intensities of the spots. As a powerful inhibitor of apoptosis and caspase activation, α1-antitrypsin inhibits many of the proteases that are released from dying cells, and thus protects normal tissues during periods of stress, such as inflammation [9]. The observed increases in the α1-antitrypsin levels of the post-treatment sera may represent self-protective responses of the liver. Although Steel *et al.* [8] found that a fragment of complement C3 was downregulated in HCC, we identified complement C3 as being upregulated after RFA treatment. This could indicate recovery of the liver, although more study is necessary.

As shown in Table 1, the types of tumor markers produced by HCC differ among patients, and neither the sensitivity nor the specificity of the three markers is satisfactory. As the sample number was small and the patients had different etiological backgrounds, the clinical significance of the proteins identified here must be explored by analyzing more cases. We propose an analytical procedure using a standard statistical algorithm [14] with carefully normalized and transformed data [13] in combination with protein identification using TOF/TOF technology.

As previously described, AFP, L3, and DCP are frequently used clinical HCC tumor markers. L3, which is a fucosylated fraction of AFP, is considered more specific than AFP for HCC. We tried to evaluate the degrees of differences in individuals around the time of treatment using these three HCC markers, but it proved too difficult. Albumin is a carrier protein for many small proteins and peptides, is one of the most abundant proteins, and has an M_r of 69 kDa and a p*I* value of 6. Different forms of modified/processed albumin appear and form multiple spots in the 2-DE gel, which leave traces that make it difficult to detect spots with a p*I* value lower than 6. AFP, the L3 fraction, and DCP are positioned in this area, and it is technically difficult to identify these proteins on gels.

In the final analysis, we identified 45 of the 812 protein spots on the 2-DE gels using MS/MS. As listed in Table 2, many of these identified spots represented PTM variants; they collapsed into 15 distinct proteins after homology and similarity searches eliminated redundant protein annotations (indicated as asterisks in Fig. 3B, and Table 2).

The technique of comparative proteomics is an effective platform for the study of cancer. The 2-DE images presented in this study will facilitate the identification of potential tumor markers and increase our understanding of the mechanisms of HCC.

This work was supported by a research grant from the Ministry of Culture, Science, and Sports. We thank Mitsuko Tsubouchi for technical assistance.

5 References

[1] Kew, M. C. *et al.*, *Sleisenger and Fordtran's Gastrointestinal and Liver Disease*, W. B. Saunders, Philadelphia 1998, pp. 1577–1602.

[2] El-Serag, H. B., Mason, A. C., Key, C., *Hepatology* 2001, *33*, 62–65.

[3] Shiina, S., Teratani, T., Obi, S., Hamamura, K. *et al.*, *Oncology* 2002, *62 Suppl 1*, 64–68.

[4] Livraghi, T., *Eur J Ultrasound* 2001, *13*, 167–176.

[5] Omata, M., Yoshida, H., Shiratori, Y., Shiina, S., *J. Gastroenterol. Hepatol.* 2002, *17 Suppl 3*, S434–S436.

[6] Wulfkuhle, J. D., Liotta, L. A., Petricoin, E. F., *Nat. Rev. Cancer* 2003, *3*, 267–275.

[7] Petricoin, E. F., Liotta, L. A., *Curr. Opin. Biotechnol.* 2004, *15*, 24–30.

[8] Steel, L. F., Shumpert, D., Trotter, M., Seeholzer, S. H. *et al.*, *Proteomics* 2003, *3*, 601–609.

[9] He, Q. Y., Lau, G. K., Zhou, Y., Yuen, S. T. *et al.*, *Proteomics* 2003, *3*, 666–674.

[10] Medzihradszky, K. F., Campbell, J. M., Baldwin, M. A., Falick, A. M. *et al.*, *Anal. Chem.* 2000, *72*, 552–558.

[11] Bienvenut, W. V., Deon, C., Pasquarello, C., Campbell, J. M. *et al.*, *Proteomics* 2002, *2*, 868–876.

[12] Blum, H., Beier, H., Gross, H. J., *Electrophoresis* 1987, *8*, 93–99.

[13] Quackenbush, J., *Nat. Genet.* 2002, *32 Suppl*, 496–501.

[14] Eisen, M. B., Spellman, P. T., Brown, P. O., Botstein, D., *Proc. Natl. Acad. Sci. U S A* 1998, *95*, 14863–14868.

[15] Katayama, H., Nagasu, T., Oda, Y., *Rapid Commun. Mass Spectrom.* 2001, *15*, 1416–1421.

[16] Bienvenut, W. V., Sanchez, J. C., Karmime, A., Rouge, V. *et al.*, *Anal. Chem.* 1999, *71*, 4800–4807.

[17] Kawakami, T., Chiba, T., Suzuki, T., Iwai, K. *et al.*, *EMBO J.* 2001, *20*, 4003–4012.

[18] Bosch, F. X., Ribes, J., Borras, J., *Semin. Liver Dis.* 1999, *19*, 271–285.

[19] Parkin, D. M., Pisani, P., Ferlay, J., *Int. J. Cancer* 1999, *80*, 827–841.

[20] Scopes, R. K., *Protein Purification: Principles and Practice*, Springer-Verlag, New York1994.

[21] Yamashita, T., Kaneko, S., Hashimoto, S., Sato, T. *et al.*, *Biochem. Biophys. Res. Commun.* 2001, *282*, 647–654.

[22] Shirota, Y., Kaneko, S., Honda, M., Kawai, H. F. *et al.*, *Hepatology* 2001, *33*, 832–840.

[23] Xu, X. R., Huang, J., Xu, Z. G., Qian, B. Z. *et al.*, *Proc. Natl. Acad. Sci. U S A* 2001, *98*, 15089–15094.

[24] Graveel, C. R., Jatkoe, T., Madore, S. J., Holt, A. L. *et al.*, *Oncogene* 2001, *20*, 2704–2712.

[25] Wirth, P. J., *Electrophoresis* 1994, *15*, 358–371.

[26] Yu, L. R., Zeng, R., Shao, X. X., Wang, N. *et al.*, *Electrophoresis* 2000, *21*, 3058–3068.

[27] Peebles, K. A., Duncan, M. W., Ruch, R. J., Malkinson, A. M., *Carcinogenesis* 2003, *24*, 651–657.

[28] Tso, P., Liu, M., Kalogeris, T. J., Thomson, A. B., *Annu. Rev. Nutr.* 2001, *21*, 231–254.

[29] Vergnes, L., Taniguchi, T., Omori, K., Zakin, M. M. *et al.*, *Biochim. Biophys. Acta.* 1997, *1348*, 299–310.

Available online at www.sciencedirect.com
SCIENCE DIRECT®
Journal of Steroid Biochemistry & Molecular Biology 94 (2005) 303–309
The Journal of Steroid Biochemistry & Molecular Biology
www.elsevier.com/locate/jsbmb

HX531, a retinoid X receptor antagonist, inhibited the 9-cis retinoic acid-induced binding with steroid receptor coactivator-1 as detected by surface plasmon resonance

Toshie Kanayasu-Toyoda, Tomofumi Fujino, Tadashi Oshizawa, Takayoshi Suzuki, Tomoko Nishimaki-Mogami, Yoji Sato, Jun-ichi Sawada, Kazuhide Inoue, Koichi Shudo, Yasuo Ohno, Teruhide Yamaguchi*

National Institute of Health Sciences, 1-18-1, Kamiyoga, Setagaya-ku, 158-8501 Tokyo, Japan

Received 3 September 2004; accepted 29 November 2004

Abstract

HX531 is a retinoid X receptor (RXR) antagonist that inhibits 9-cis retinoic acid-induced neutrophilic differentiation of HL-60 cells. In order to elucidate the inhibitory mechanism of HX531, we have developed a novel ligand sensor assay for RXR in which the receptor–coactivator interaction is directly monitored using surface plasmon resonance (SPR) biosensor technology. A 20-mer peptide from steroid receptor coactivator-1 (SRC-1), containing nuclear receptor interaction motif LXXLL was immobilized on the surface of a BIAcore sensor chip. Injection of human recombinant RXR with or without 9-cis retinoic acid resulted in ligand-dependent interaction with the SRC-1 peptide. Kinetic analysis revealed dissociation constants (KD) of 9-cis RA-preincubated RXR to SRC-1 was 5.92×10^{-8} M. Using this technique, we found that 1 μM HX531 reduced the ka value of liganded-RXR with SRC-1, suggesting that HX531 reduced the affinity of RXR to SRC-1. This SPR assay system was applied to obtain quantitative kinetic data of RXR ligand binding to the SRC-1 peptide and the alteration of these data by antagonists.

Keywords: Retinoid X receptor; Steroid receptor coactivator-1; 9-cis Retinoic acid; HX531; PA024; HL-60 cells; Surface plasmon resonance

1. Introduction

Retinoids have a chemopreventive and therapeutic potency in oncology and dermatology. All-trans retinoic acid (ATRA) and 9-cis retinoic acid (9-cis RA) are well- known natural retinoids. Retinoidal activities are mainly achieved through the transcriptional regulations of specific genes via two kinds of nuclear receptors (NRs): (a) RARα, β and γ, and (b) RXRα, β and γ. ATRA binds RARs and 9-cis RA to both RARs and RXRs.

HL-60 cells, which are an established cell line from an acutely promyelocytic leukemia patient [1], differentiate into neutrophilic cells in response to both ATRA [2] and 9-cis RA [3]. This differentiation ability of HL-60 cells has been useful for screening of chemically synthesized agonists or antagonists of NRs; HX531 was discovered as an antagonist of RXRs from the synthetic chemical library in this screening system [4]. Since HX531 inhibits the activation of both RXR homodimer and the RAR/RXR heterodimer, HX531 is expected to modulate the gene expression through these NRs. The precise mechanism of antagonistic effects by this compound, however, has not been fully elucidated.

The p160 steroid receptor coactivator (SRC) gene family contains three homologous members, which serve as transcriptional coactivators for NRs and certain other transcription factors [5]. These coactivators interact with ligand-bound NRs to recruit histone acetyltransferases (HAT) and methyl-

Abbreviations: 9-Cis RA, 9-cis retinoic acid; ATRA, all-trans retinoic acid; NRs, nuclear receptors; RXR, retinoid X receptor; rhRXR, recombinant human RXR; SRC-1, steroid receptor coactivator-1; SPR, surface plasmon resonance; RU, resonance unit; KD, dissociation constants; ka, association rate constant

* Corresponding author. Tel.: +81 3 3700 9373; fax: +81 3 3700 9373.
E-mail address: yamaguch@nihs.go.jp (T. Yamaguchi).

0960-0760/$ – see front matter © 2005 Elsevier Ltd. All rights reserved.
doi:10.1016/j.jsbmb.2004.11.007

transferases to specific enhancer/promotor regions, which in turn facilitates chromatin-remodeling [6,7], assembly of general transcription factors, and transcription of target genes. The relatively conserved central region of the SRC family contains three LXXLL motifs that are responsible for interaction with ligand-bound NRs [8–11]. Recently, it was reported that 9-cis RA-liganded RAR/RXR showed enhanced binding with SRC-1 [12]. Hence, we suspected that a binding assay utilizing liganded-RXR with SRC-1 would be useful for the analysis of RXR kinetic parameters.

HX531 inhibited the increase in the nitro blue tetrazolium (NBT) reduction ability of HL-60 cells induced by 9-cis RA [4]. In this study, we have examined the antagonistic effect of HX531 against 9-cis RA on cell growth and on expression of the formyl-Met-Leu-Phe receptor (fMLP-R) and CD11b on HL-60 cells. Furthermore, we have developed an analytical method for agonist or antagonist effects on RXR using surface plasmon resonance (SPR) biosensor technology. Here, we also discuss the interaction of SRC-1 and RXR incubated with 9-cis RA and HX531 using this new method.

2. Materials and methods

2.1. Materials

Biotinylated peptides (>95% of purity) were purchased from Biologica (Nagoya, Japan). Recombinant human RXRβ (rhRXRβ) was obtained from Affinity BioReagents (Golden, Co). 9-Cis RA and anti-human CD11b monoclonal antibody were from Sigma Chemical (St. Louis, MO) and DAKO (Glostrup, Denmark), respectively.

2.2. Cell culture and neutrophilic differentiation in relation to neutrophilic granulocytes lineage

HL-60 cells were kindly supplied by the Japanese Collection of Research Resources Cell Bank. Cells were maintained in RPMI 1640 medium, containing 10% heat-inactivated FBS and 30 mg/L kanamycin sulfate at 37 °C under moisturized air, containing 5% CO_2. HL-60 cells were differentiated into neutrophilic cells by addition of 9-cis RA. HX531 was preincubated with cells for 30 min before addition of 9-cis RA. Five days after addition of the differentiating agent, expressions of both fMLP-R and CD11b, and cell numbers were measured.

2.3. fMLP-R and CD11b expression

The differentiated cells were collected and incubated with FITC-conjugated fMLP or phycoerythrin-conjugated anti-CD11b antibody, and then labeled cells were subjected to flow cytometric analysis (FACSCalibur, Becton and Dickinson).

2.4. SPR assay

The measurements were performed using a BIAcore 3000 (BIAcore AB, Uppsala, Sweden) at 25 °C in a running buffer comprising 0.2% bovine serum albumin, 50 mM Tris–HCl (pH 7.5), 150 mM NaCl, 10 mM $MgCl_2$ and 0.1% Tween 20. Streptoavidin chips (BIAcore AB) were first treated with three 1-min pulses of 50 mM NaOH, containing 1 M NaCl at a flow rate of 10 μl/min. Wild-type peptide from human SRC-1 (wtSRC-1, CPSSHSSLTARHKILHRLLQEGSPS-CONH2, residues 676–700), containing the consensus NR interaction motif (LXXLL), and the consensus-mutated SRC-1 peptide (mtSRC-1, CPSSHSSLTARHKIAHRALQEGSPS-CONH2) were biotinylated and immobilized on individual surfaces. Recombinant human RXRβ dissolved in the running buffer was preincubated with 9-cis RA or PA024, an agonist of RXRs, in either the presence or absence of HX531 at room temperature for 1 h, and then injected over the surfaces at a flow rate of 10 μl/min. Ligands were dissolved in ethanol and the final concentration of ethanol was adjusted to 1.0%. After the injection was completed (300 s), the formed complex was washed with the running buffer for an additional 300 s. The chip surfaces were regenerated down to the peptide level by subsequent washing for 60 s pulses with 0.1% SDS and 3.3 mM EDTA solution and 10 mM NaOH solution. Ligand-treated RXR interaction with SRC-1 was represented by resonance unit (RU). Both the KD and ka values were calculated from the experimental curve with BIAcore evaluation 3.1 software package. The formation of surface-bound complexes was analyzed according to the interaction type of $A + B \leftrightarrow AB$.

2.5. Statistical analysis

Each experiment was repeated three or more times, and representative data are indicated. Statistical analysis was performed using the unpaired t-test. Values of $P < 0.05$ were considered to indicate statistical significance.

3. Results

3.1. Effects of HX531 on proliferation and CD11b and fMLP-R expression of 9-cis RA-treated HL-60 cells.

To confirm the antagonistic effects of HX531, we examined the effects of 1.0 μM HX531 on the growth of 0.1 μM 9-cis RA-treated HL-60 cells 5 days after cultivation. As shown in Fig. 1A, HX531 could not completely restore but partially antagonized the inhibitory effect of 9-cis RA on proliferation of HL-60.

The expression of fMLP-R is one of suitable maker, since we have previously reported that it positively correlated the differentiation of HL-60 cells, i.e. migration and superoxide producing abilities [13–15]. Next, the expression of both fMLP-R and CD11b was analyzed by flowcytometry 5 days

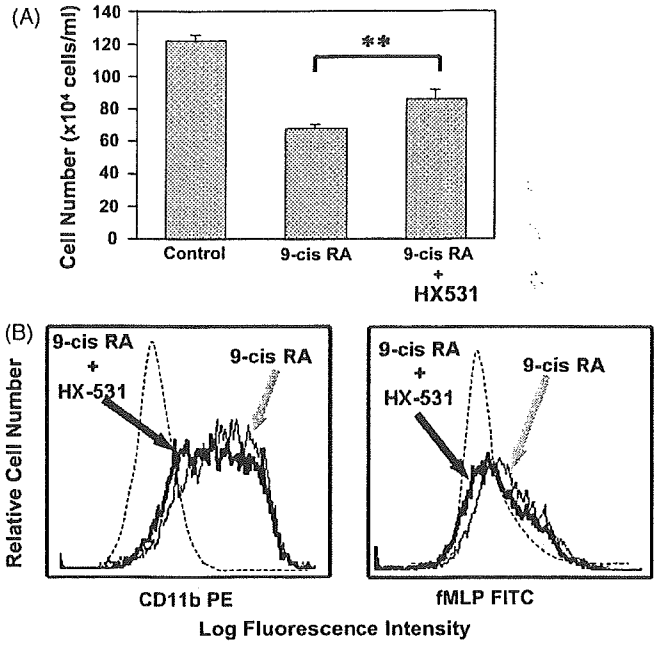

Fig. 1. Effects of HX531 on 9-cis RA-induced-proliferation and differentiation. (A) HL-60 cells were treated HX531 and 9-cis RA. Five days after treatment, cellular number was determined. Columns and bars represent the mean ± S.D. of triplicate wells (**, $P<0.01$). (B) fMLP-R and CD11b expression were analyzed by flow cytometry. Non-treated cells are indicated by dotted lines. The gray arrow indicates cells cultured with 9-cis RA (gray lines) and the black arrow the cells cultured with 9-cis RA in the presence of HX531 (black lines).

after addition of 9-cis RA in the presence or absence of HX531 (Fig. 1B). HX531 reduced not only CD11b expression but also fMLP-R expression compared with 9-cis RA-treated HL-60 cells. These results confirmed the antagonistic effects of HX531 on 9-cis RA-induced neutrophilic differentiation and growth arrest.

3.2. Establishment of SPR assay and inhibitory effects of HX531

To elucidate the antagonistic effects of HX531 against 9-cis RA, we undertook establishment of an SPR assay system using the ligand-dependent interaction of NRs and SRCs. First, we tried to detect the signals of ligand-dependent RXR binding with SRC-1 using SPR. When rhRXRβ was injected over the sensor chip surface immobilized with a 20-mer peptide, containing the NR interaction consensus motif LXXLL of SRC-1 (wtSRC-1), a small response was observed in the absence of 1 μM 9-cis RA (Fig. 2A, upper panel; 0.225 μM (−)). The signal observed from the injection of 0.225 μM rhRXRβ was markedly enhanced by preincubation with 9-cis RA (+) compared with control (−), and the signal increased with rhRXRβ in a dose-dependent fashion. On the other hand, when mutated SRC-1 peptide (mtSRC-1), containing alanine substitutions in the core motif (AXXAL) was immobilized on the sensor chip surface as a control, only a very weak signal was observed (Fig. 2A, lower panel) compared to that of wtSRC-1 peptide. Thus, these data indicated that the 9-cis RA-elicited signal observed in the injection of RXR with the SRC-1 peptide was specific to the LXXLL motif.

Table 1

Treatment (μM)	HX531 (±1 μM)	ka ($\times 10^3\ M^{-1}\ s^{-1}$)
Control		
	−	0.50
	+	0.18
PA024		
10.0	−	4.89
1.0	−	3.41
1.0	+	2.40
9-cis RA		
10.0	−	2.16
1.0	−	1.45
1.0	+	1.08

The ka values of rhRXRβ treated with PA024 and 9-cis RA in the presence or absence of HX531.

To obtain the sensorgrams showing the LXXLL motif-specific interaction, we subtracted the sensorgrams using mtSRC-1 peptide from those produced by the wtSRC-1 peptide in the following experiments. The result by sensorgrams (Fig. 2B) clearly shows the specific binding of liganded-RXR to the SRC-1 peptide, and the kinetic analysis established an association constant (KA) for 9-cis RA-preincubated RXR of $1.69 \times 10^7\ M^{-1}$, which was three-fold greater than its dissociation constants (KD, 5.92×10^{-8} M).

Next, rhRXR was incubated with PA024 (1 μM or 10 μM) or 9-cis RA (1 μM or 10 μM), and then the incubation mixture was subjected to SPR analysis subtracting the sensorgrams using mtSRC-1 peptide from those produced by the wtSRC-1. In this analysis, the concentration of the rhRXR protein was fixed at 0.9 μM (Fig. 3A), and the association rate constant (ka) from liganded-RXR binding with SRC-1 was calculated. The addition of 1 μM and 10 μM of PA024 markedly increased the ka from $0.5 \times 10^3\ M^{-1}\ s^-$ in the control to $3.41 \times 10^3\ M^{-1}\ s^-$ and $4.89 \times 10^3\ M^{-1}\ s^-$, respectively. 9-cis RA (1 μM and 10 μM) also increased the ka value to $1.45 \times 10^3\ M^{-1}\ s^-$ and $2.16 \times 10^3\ M^{-1}\ s^-$, respectively, although the KD value of RXR did not change. These data indicate that RXR agonists caused an increase in the binding of RXR to SRC-1 in this system. The binding of RXR to the SRC-1 peptide may increase due to ligand presence in a dose-dependent manner.

When rhRXRβ was preincubated with (HX) or without (control) 1 μM HX531 alone, no signal difference was observed (Fig. 3B), suggesting that HX531 dose not affect the ligand-independent binding of rhRXRβ to SRC-1 peptide. When rhRXRβ was incubated with either 1 μM PA024 or 1 μM 9-cis RA in the presence of HX531, the signals were reduced compared with those in the absence of HX531 (Fig. 3B). All ka values are shown in Table 1. These results indicated that it is possible to analyze the kinetics parame-